# Substituted [Cu(I)(POP)(bipyridyl)] and related complexes: Synthesis, structure, properties and applications to dye-sensitised solar cells†‡

**Charlotte L. Linfoot, Patricia Richardson, Tracy E. Hewat, Omar Moudam, Michael M. Forde, Anna Collins, Fraser White and Neil Robertson***

***Received 23rd March 2010, Accepted 8th July 2010***
**DOI: 10.1039/c0dt00190b**

The synthesis and subsequent spectroscopic, electrochemical, photophysical and computational characterisation of a series of heteroleptic Cu(I) complexes of general formula: [CuPOP{*4*,*4′*(R)-bipyridyl}][$BF_4$] and [CuPOP{*4*,*4′*,*6*,*6′*(R)-bipyridyl}][$BF_4$] is described (POP = bis{2-(diphenylphosphanyl)phenyl} ether; R = Me, $CO_2H$, $CO_2Et$. The steric constraint imposed by the POP ligand can impede distortion towards square planar geometry upon MLCT excitation or oxidation and this is explored in the context of varying substituents on the bipyridyl ligand. The insight gained opens new avenues for design of functional Cu(I) systems suitable for photophysical and photoelectrochemical applications such as sensitisers for dye-sensitised solar cells (DSSCs).



## Introduction

Recent research into the electrochemical and photophysical properties of phenanthroline- and bipyridine-based Cu(I) complexes[1–4] has revealed their potential for application in dye-sensitised solar cells (DSSCs),[2,3,5–7] organic light emitting diodes (OLEDs)[4,8] and light-emitting electrochemical cells (LECs).[4,8] The most successful DSSCs developed to date are based on Ru(II) containing sensitiser molecules,[9] some of which are being commercially developed for niche markets.[10] Lower efficiency DSSCs have also been constructed using transition metal complexes of Os(II), Pt(II), Re(I), Cu(I), Fe(II)[11] and Ni(II).[12] The use of third row transition metal sensitisers has been particularly successful due to their ability to display long-lived excited states following MLCT absorption in the visible. However low abundance, and toxicity considerations could present detrimental practical implications in the long term. Research into the field of first row transition metals has been limited due to their often extremely short-lived excited states compared to 2nd and 3rd row transition metal complexes, arising from the low lying metal d-d excited states which allow non-radiative decay of the MLCT excited state. This is a limiting factor in terms of DSSC functionality as charge injection from the dye is not efficiently achieved.[13,14]

To overcome this problem, complexes with a strong crystal field have been studied, aimed at raising the energy of any d-d excited states. This strategy has been explored by Ferrere[13,15,16] with work on Fe(II) sensitiser molecules analogous to known Ru(II) sensitisers that exhibit strong crystal-field splitting.[9] Solar cell function was observed but it was significantly reduced compared to the corresponding Ru(II) sensitiser. Similarly low efficiencies using Ni(II)(dithiolate)(diimine) complexes as DSSC sensitiser molecules has recently been presented by our group, with limited solar cell function being observed,[12] also attributed to short excited state lifetimes.

In contrast, Cu(I) complexes can display longer excited-state lifetimes due to their $d^{10}$ configuration, leading to a power-conversion efficiency of 2.6%.[17] To date however, Cu(I) DSSC research has been limited to homoleptic sensitisers,[2,3,5,7] and in this work we extend this to an initial investigation of heteroleptic Cu(I) complexes. In analogous Ru(II) dyes, the heteroleptic ligands control directionality of the MLCT transition to minimise recombination losses and also allow tuning of the HOMO energy.[18] During the redox process; Cu(I)/Cu(II),[19,20] a conformational geometry change typically occurs from distorted tetrahedral to tetragonally-flattened, respectively.[21] Research investigating Cu(I) bis-phenanthroline complexes[1,8,20–22] has revealed that substituents in the 2- and 9-positions of the phenanthroline ligand acts as "blocking groups" to sterically constrain the molecule.[1,20,21] A similar approach has been utilised for DSSC Cu(I) sensitisers by including substituents groups in the 6,6′positions of the bipyridine, however this leads to increased synthetic complexity of the bipyridine ligands which must also be 4,4′-substituted with acid groups to bind to $TiO_2$.[2,3,5–7] In this work, we

*School of Chemistry and EaStChem, University of Edinburgh, King's Buildings, Edinburgh, UK. E-mail: neil.robertson@ed.ac.uk; Fax: +44 131 6504743; Tel: +44 131 650 4755*

†

‡ Electronic supplementary information (ESI) available: Figure A. Schematic of the POP chelate ring; Figure B. Mercury plots of [Cu(dmbpy)$_2$Cl][$BF_4$] demonstrating π–stacking interactions; Figure C. Mercury plots of **1** demonstrating no π–stacking interactions; Figure D. (a) Absorbance Spectra for **1** and **3**; (b) Absorbance Spectra for **4**, **6**, **7** and **9**; Figure E. Excitation and Emission Spectra; Figure F. Selected Molecular Orbital Images for **4**; Figure G. Selected Molecular Orbital Images for **5**; Figure H. Selected Molecular Orbital Images for **7**; Figure I. Selected Molecular Orbital Images for **9**; Figure J. Molecular Orbital Diagram for **4**; Figure K. Molecular Orbital Diagram for **7**; Figure L. Molecular Orbital Diagram for **5**; Figure M. *I–V* Curve for **5**; Figure N. *I–V* Curve for **5** with Cheno treatment; Figure O. *I–V* Curve for **5** with $TiCl_4$ treatment; Table A. Crystallographic data for complexes **6**, **9** and **10**; Table B. Percentage contributions from component parts of **4** to selected molecular orbitals; Table C. TDDFT calculated visible absorption wavelengths for **4**; Table D. Percentage contributions from component parts of **5** to selected molecular orbitals; Table E. TDDFT calculated visible absorption wavelengths for **5**; Table F. Percentage contributions from component parts of **7** to selected molecular orbitals; Table G. TDDFT calculated visible absorption wavelengths for **7**; Table H. Percentage contributions from component parts of **9** to selected molecular orbitals; Table I. TDDFT calculated visible absorption wavelengths for **9**. CCDC reference numbers 771439–771443. For ESI and crystallographic data in CIF or other electronic format see DOI: 10.1039/c0dt00190b

explore the use of a geometrically inflexible co-ligand bis{2-(diphenylphosphanyl)phenyl} ether (POP), enabling the simpler 4,4′-$(CO_2H)_2$-bipyridine to be used as the $TiO_2$-binding ligand, without requiring 6,6′-substitution and therefore simplifying the intensive bipyridine synthesis required for previous Cu(I)-based sensitisers. POP has been used effectively in OLED studies due to this rigid and inflexible geometry it can impose on the complex.[13,23,24]

The work outlined here reports the synthesis and subsequent electrochemical and photophysical characterisation of a series of homo- and heteroleptic Cu(I)(bipyridine) complexes (Fig. 1 and 2), enabling a comparison of structural rigidity imposed by the POP and variously-substituted bipyridine ligands. Included is the first example of a heteroleptic Cu(I) complex investigated as a DSSC sensitiser.

## Results and discussion

### Syntheses

The ligands 4,4′-dicarboxy-2,2′-bipyridine (dcbpy), 4,4′-di($CO_2Et$)-2,2′-bipyridine (decbpy), 4,4′,6,6′-tetramethyl-2,2′-bipyridine (tmbpy) and bis{2-(diphenylphosphanyl)phenyl} ether (POP), and the starting complexes $[Cu(MeCN)_4][BF_4]$ and $[Cu(POP)(MeCN)_2][BF_4]$ were synthesised using modified literature methods as described in the Experimental section. 4,4′,6,6′-tetracarboxy-2,2′-bipyridine (tcbpy) and 4,4′,6,6′-tetra($CO_2Et$)-2,2′-bipyridine (tecbpy) are novel ligands that were synthesised *via* oxidation of the tmbpy ligand. The reaction schemes shown in Fig. 1 and 2 demonstrate how the Cu(I) complexes were synthesised by simple addition, with stirring, of the relevant starting materials in stoichiometric amounts, to the appropriate solvent at room temperature. It should be noted that $[Cu(tcbpy)_2][BF_4]$ **2**, and $[Cu(POP)(tcbpy)][BF_4]$ **8** were synthesised and characterised by $^1H$ NMR under nitrogen, but were not air stable and so were not further investigated. The methyl and ester analogues have been synthesised alongside the acids, despite not being directly applicable for use in a DSSC, as they can give insight into the properties of the acid complexes while being more convenient for detailed characterisation due to better solubility. The Cu(I) complexes **1**, **3**–**7** and **9** were characterised by $^1H$ NMR, ESI-MS, +FAB-MS and elemental analysis, verifying molecular structures.

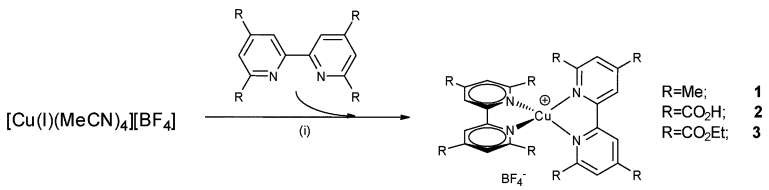


**Fig. 1** Synthetic reaction scheme for homoleptic complexes reported in this work. All procedures carried out under a nitrogen atmosphere. (i) **1** degassed chloroform; **2** dry, degassed MeOH; **3** dry, degassed DCM.

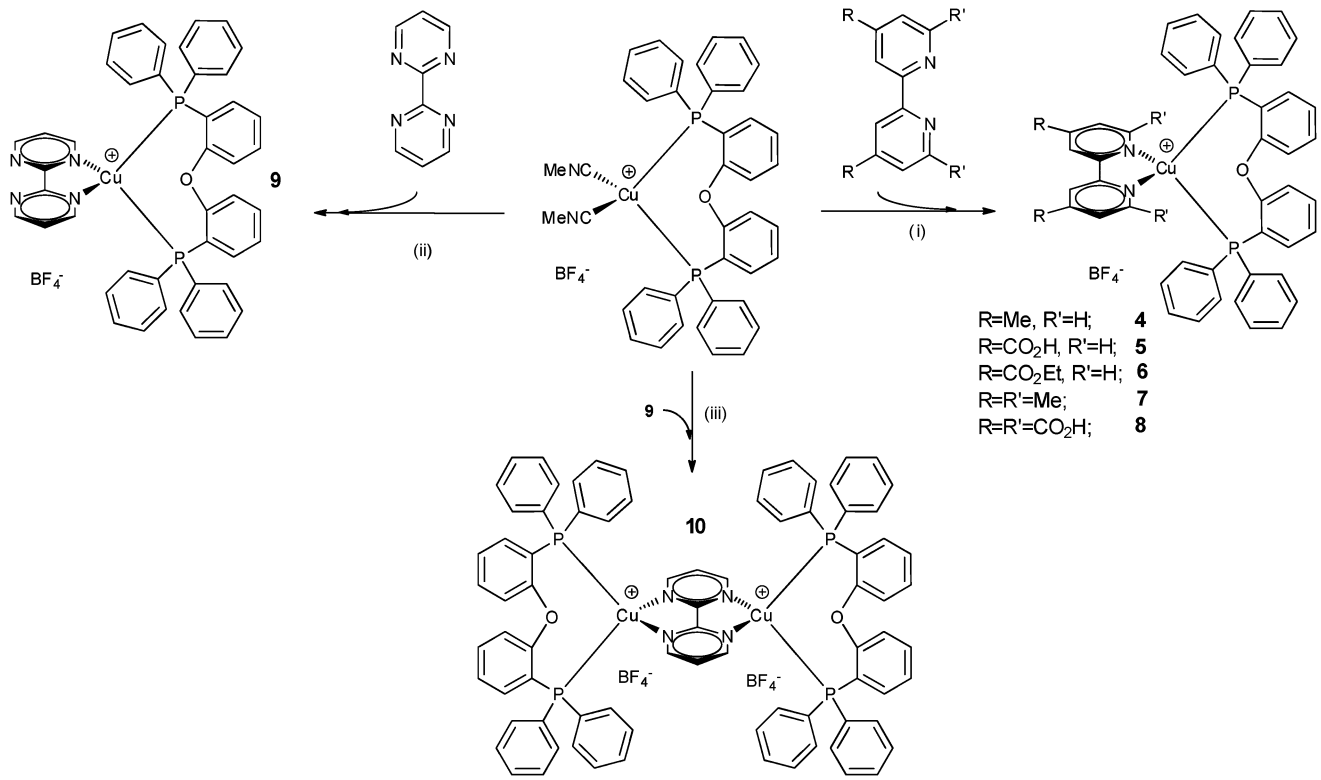


**Fig. 2** Synthetic reaction scheme for heteroleptic complexes reported in this work. (**1**) **4**, **5**, **6**, **8** acetone; **7** anhydrous acetonitrile (ii) DCM (iii) acetone.

 

**Table 1** Selected bond lengths (Å) and bond angles (deg) of complexes $[Cu(dmbpy)_2Cl][BF_4]$ and **1**

| | $[Cu(dmbpy)_2Cl][BF_4]$ | **1** |
|---|---|---|
| Cu–N(1A) | 2.154(2) | 2.055(2) |
| Cu–N(1B) | 2.082(2) | 2.056(2) |
| Cu–N(2A) | 2.001(2) | 2.055(2) |
| Cu–N(2B) | 1.981(2) | 2.056(2) |
| N(1A)–Cu–N(1B) | 100.97(8) | 117.63(9) |
| N(2A)–Cu–N(2B) | 169.34(8) | 117.63(9) |
| N(1A)–Cu–N(2B) | 91.78(8) | 134.37(9) |
| N(2A)–Cu–N(1B) | 96.60(8) | 134.37(9) |
| N(1A)–Cu–N(2A) | 79.07(8) | 80.60(13) |
| N(1B)–Cu–N(2B) | 79.64(8) | 80.63(13) |

## Structure analysis

The single crystal structures of $[Cu(II)(dmbpy)_2Cl][BF_4]$ and compounds **1**, **6**, **9** and **10** have been determined allowing insight into the structural features of these complexes (Table 1 and 2), in particular the blocking group effects. All crystals were grown from solutions open to air. Despite obtaining a crystal structure of **10**, we were unable to isolate the complex in a pure form and therefore further characterisation was not carried out. In attempting to crystallise the 4,4′-dimethyl-2,2′-bipyridine analogue of **1**, the complex oxidised in air along with coordination of chlorine to give $[Cu(II)(dmbpy)_2Cl][BF_4]$ (Fig. 3a). In contrast, the structure of complex **1** (Fig. 3b) illustrates the stabilisation of the Cu(I) oxidation state by addition of methyl groups in the 6,6′-positions of the bipyridine. The angle between the planes of the two bipyridyls is 72.18° giving a pseudo-tetrahedral geometry and suggesting considerable flexibility of this geometric parameter.

The crystal structures of the heterolpetic complexes (**6**, **9** and **10**) shown in Fig. 4 illustrate the role of POP in stabilisation in air of a Cu(I) oxidation state over Cu(II) as the complexes are forced to adopt distorted tetrahedral conformations with reduced structural flexibility. The angles between the bipyridyl plane and the P–Cu–P plane for these complexes range from 84.05 to 88.61° indicating a geometry closer to tetrahedral than that of **1** (Table 2). Additionally, the bite angle of POP in each case remains comparatively close to that expected for an ideal tetrahedron (Table 2). The blocking functionality of POP arises as one of

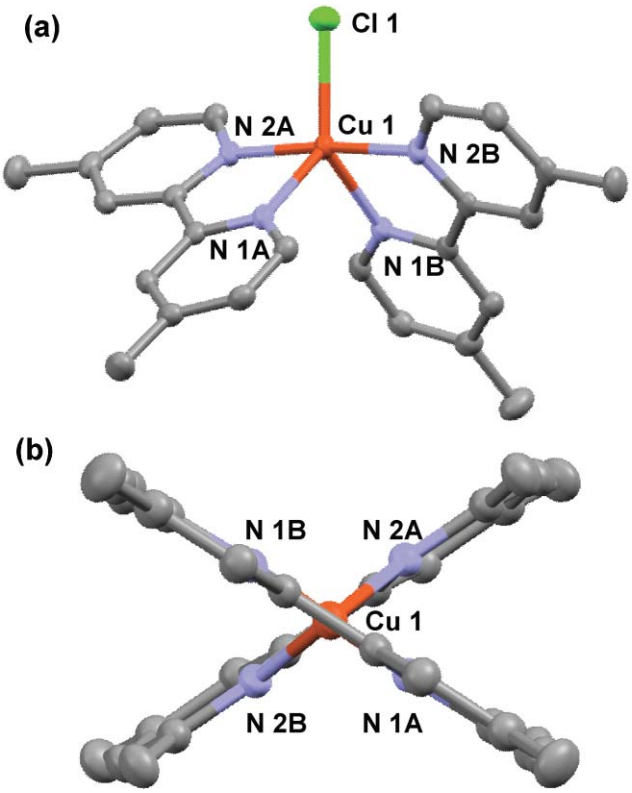


**Fig. 3** Mercury plots of (a) $[Cu(dmbpy)_2Cl][BF_4]$; and (b) **1**. Thermal ellipsoids are drawn at the 50% probability level. $[BF_4]$ counter ion omitted for clarity. Selected bond lengths and bond angles for $[Cu(dmbpy)_2Cl][BF_4]$ involving the chloride atom: Cu–Cl: 2.2770(7) Å; Cl–Cu–N(1A) 123.54(6)°; Cl–Cu–N(2A) 93.08(6)°; Cl–Cu–N(1B) 135.48(6)°; Cl–Cu–N–(2B) 96.57 (6)°.

the phenyl rings attached to the phosphorus atoms is constrained to be over the bipyridyl ligand resulting in H-phenyl-to-bipyridyl plane distances of 2.891 Å, 2.941 Å, 2.790 Å for **6**, **9** and **10** respectively that prevent structural distortion. This geometrical arrangement is caused by the rigid nature of the chelating ring (Cu–P–C–C–O–C–C–P). Among the three structures presented here (see supplementary information) and also those reported

**Table 2** Selected bond lengths (Å) and bond angles (deg) from single crystal X-ray crystallography for **6**, **9** and **10**.; and from solvated DFT calculations for **9**

X

| | **6** | **9**: single crystal X-ray structure | **9**: DFT geometry optimisation | **10** |
|---|---|---|---|---|
| Cu–N(1) | 2.037 (2) | 2.068(2) | 2.105 | 2.103(2) |
| Cu–N(2) | 2.0621(19) | 2.093(2) | 2.107 | 2.070(2) |
| Cu–P(1) | 2.2213(6) | 2.2482(7) | 2.400 | 2.2158(7) |
| Cu–P(2) | 2.2465 (6) | 2.2756(7) | 2.411 | 2.2851(7) |
| N(1)–Cu–N(2) | 80.30(8) | 79.74(8) | 79.64 | 80.16(8) |
| N(1)–Cu–P(1) | 128.87(6) | 121.08(6) | 121.96 | 128.91(6) |
| N(2)–Cu–P(1) | 111.47(5) | 118.49(6) | 115.30 | 119.24(6) |
| N(1)–Cu–P(2) | 109.74(6) | 108.47(6) | 106.85 | 102.14(6) |
| N(2)–Cu–P(2) | 112.26(5) | 113.65(6) | 112.25 | 102.75(6) |
| P(1)–Cu–P(2) | 110.40(2) | 111.77(2) | 114.50 | 116.30(3) |
| bpy plane–PCuP plane[a] | 84.05 | 85.77 | N/A | 88.61 |
| Cu–P(2)–C[b] | 114.38(8) | 115.58(8) | 115.89 | 107.54(9) |

[a] for **6** C═C17; for **9** C═C9; for **10** C═C35.

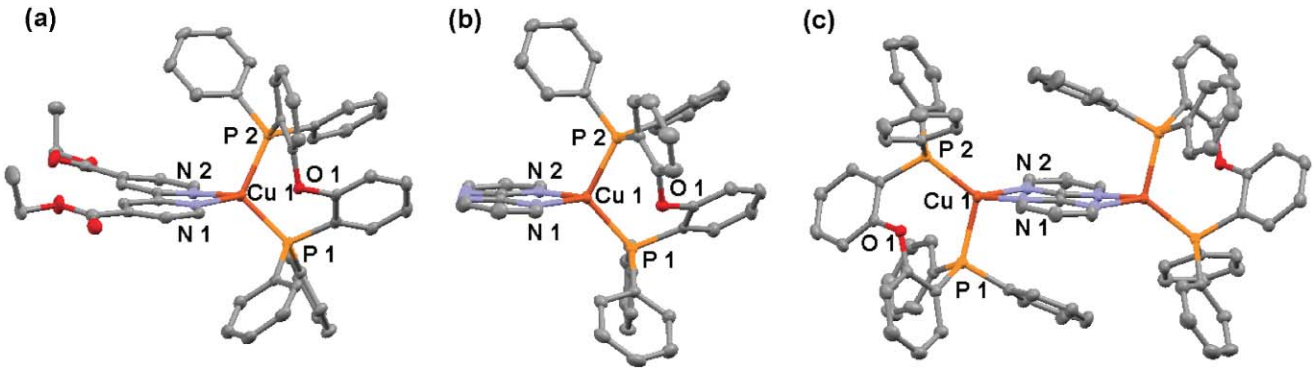


**Fig. 4** Mercury plots of (a) **6**; (b) **9** and (c) **10**. Thermal ellipsoids are drawn at the 50% probability level. **10** lies on an inversion centre. The [$BF_4$] counter ions are omitted for clarity.



previously, there is little variation between the angles within the chelate ring providing strong support for the lack of flexibility in the POP coordination geometry and hence the rigidity of the whole molecule. In general, the structures shows little geometric deviation compared with eleven POP containing Cu(I)-structures described in the literature.[14,24–28] Furthermore, the structures of **6** and **9** clearly demonstrate that in a heteroleptic complex with an appropriate co-ligand, 6,6′-substituted bipyridine ligands are not required to maintain an air-stable Cu(I)-complex. This enables the use in Cu(I) DSSC sensitisers of the straightforward dcbpy ligand widely exploited in Ru sensitisers and bypassing the need for more complex multiply substituted bipyridyl ligands.

## DFT and TDDFT calculations

All calculations were carried out using Gaussian 03[29] with the B3LYP/LANL2DZ[30–33] functional and basis set with induced solvent effects. This level of theory has been used successfully in the literature to calculate the structural and electronic properties of a number of coordination complexes.[25] Calculation details are outlined in full in the Experimental section. The optimised geometry for **9** is in very good agreement with the structure obtained crystallographically (Table 2), but as expected the DFT calculated solvated bond lengths are longer than those in the crystal structure. Packing forces present in the calculated liquid-phase are weaker than those in the solid-phase. The DFT calculated gas-phase and solution-phase structures for **4**, **5**, **7** and **9** produce identical overall structure energies and comparable bond distances and angles.

Time dependent density functional theory (TDDFT), also at the B3LYP/LANL2DZ level of theory, was used to probe the electronic transitions that give rise to the visible and near-UV absorption of each complex. Although current TDDFT implementations have a tendency to underestimate the energy of charge-transfer interactions, the method has been shown to provide useful qualitative information on the electronic structure and photophysical behaviour of similar coordination complexes.[25] Seventy singlet-singlet transitions were calculated with solvent, for each complex. Analysis of the components of the TDDFT expansion shows that the majority of predicted transitions are not well described by a single electron-promotion, but involve transitions between several different orbital pairs.

The nature of each electronic transition was determined by visual inspection (Argus Lab[34]) of each contributing molecular orbital as an isosurface map. Many of the calculated occupied and virtual orbitals were seen to be of mixed character, with electron density simultaneously present on both the ligand and metal. However, the electronic transitions could broadly be

classified into three distinct types; metal-to-ligand-charge-transfer (MLCT), where the occupied orbital is predominantly metal based and the virtual orbital ligand based, either on the POP or bpy; ligand-ligand (LL), where the transition involves occupied and virtual orbitals on the same ligand; and ligand-to-ligand-charge-transfer (LLCT), where the transition involves occupied and virtual orbitals on different ligands. These are discussed further in the context of the experimental results below.

## UV/Vis absorption spectroscopy

The experimental and calculated UV-Vis absorption spectra are shown in Fig. 5, with the main absorption bands and related extinction coefficients given in Table 3. For each complex the experimental spectra show two distinct groupings; very strong absorption in the near uv and weaker absorption bands in the visible that are sensitive to the nature of the biypridine substituents. From previous work,[1] it is known that the absorption peak of the $\pi \rightarrow \pi^*$ intra-bipyridine transition occurs between 300–320 nm. Each complex in the homoleptic series exhibits an absorption peak in this range (Table 3), however this absorption peak cannot be resolved for the heteroleptic series as it is believed to be masked by the stronger POP ligand UV absorption band. In the absorbance spectra collected for **4** and **7** the shoulder present at 320 nm may possibly be attributed to the bipryidyl absorption.

The TDDFT calculations reproduce the experimental spectra reasonably well in the UV region, predicting a large number of transitions with significant oscillator strength (Fig. 5). Examination of the molecular orbitals involved in each transition shows that the UV absorption bands are dominated by $\pi \rightarrow \pi^*$ transitions on both the bipyridine and the POP ligands (see supplementary information‡).

The longer wavelength bands have been assigned as Cu(I) to bipyridyl MLCT transfer bands based upon comparison with literature. This assignment is supported by the calculated energies and deduced characters of the frontier orbitals (Table 4) and the percentage contribution to the lowest energy MLCT bands, of

 

**Table 3** Absorbance measurements for all complexes. **1** and **4 - 9** carried out in MeCN; **3** carried out in DCM

| Complex | | Absorption/$\lambda_{max}$/nm ($\varepsilon_{max}$($\times 10^3$ $M^{-1}cm^{-1}$)) | | | | |
|---|---|---|---|---|---|---|
| | | Intraligand transitions | | | MLCT | |
| [Cu(tmbpy)$_2$] | **1** | | | 300 (25.8) | 358 (1.4) | 449 (3.5) |
| [Cu(tecbpy)$_2$] | **3** | | | 315 (32.0) | 477 (4.9) | 594 (7.4) |
| [CuPOP(MeCN)2] | — | | 272 (14.2) | | | |
| [CuPOP(dmbpy)] | **4** | 248 (25.1) | 282 (22.6) | | 369 (3.2) | |
| [CuPOP(dcbpy)] | **5** | | 276 | | 416 | |
| [CuPOP(decbpy)] | **6** | 246 (26.6) | 290 (19.7) | | 424 (2.4) | |
| [CuPOP(tmbpy)] | **7** | 250 (26.3) | 288 (25.5) | | 358 (2.2) | 460 (0.2) |
| [CuPOP(bpym)] | **9** | 247 (35.5) | 294 (16.1) | | 403 (2.0) | |



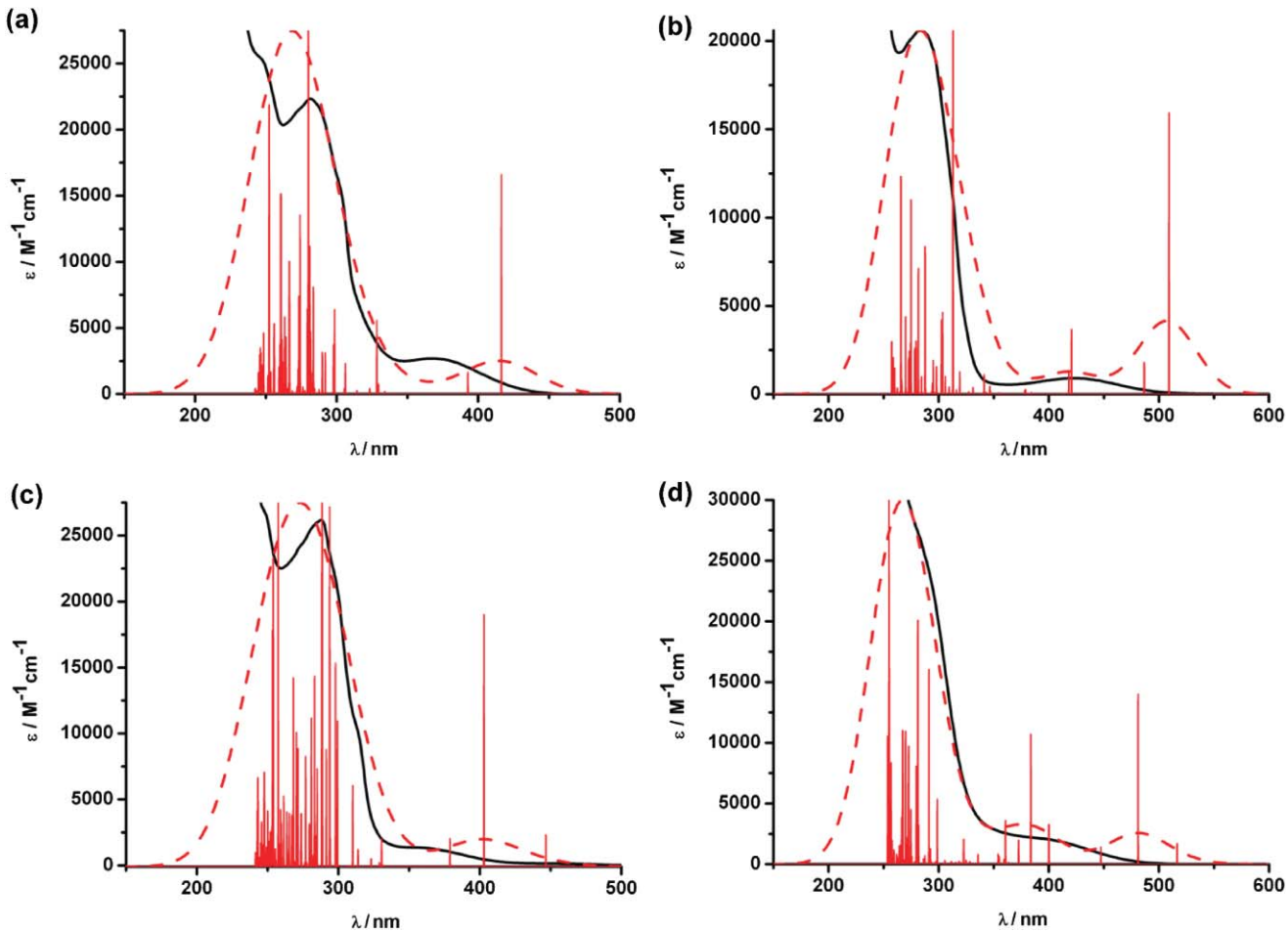


**Fig. 5** Theoretical UV/Vis absorption spectra against experimental absorption spectra for (a) **4**; (b) **5**; (c) **7**; (d) **9**.Where red solid columns = calculated electronic transition; red dotted line = calculated spectra; black solid line = solution spectrum of (a) **4**, (b) **6**, (c) **7** and (d) **9** in MeCN.

each orbital pair (Table 5) in the TDDFT expansion. It must be noted that TDDFT has a tendency to over stabilise, and indeed the calculated MLCT absorptions are consistently predicted at lower energy than those seen experimentally.[35]

For the 4,4′-disubstituted complexes the TDDFT calculations agree with experimental data in placing the MLCT absorption for **5** at lower energy than that of **4**. The proposed explanation for this, based upon the previous experimental data, is that **5** has a lower lying LUMO as a result of the electron-withdrawing acid substituents. This proposal can be further confirmed upon inspection of the TDDFT results with Fig. 6 showing molecular orbital images for the LUMO of **4** and **5**. **5** displays increased delocalisation and therefore a lower energy LUMO (Table 4) which subsequently reduces the required MLCT energy, causing the absorption to take place at longer wavelength.

The MO diagram for **4** looks almost as expected for a pseudo-tetrahedral complex (see supplementary information‡). Three MOs are close in energy (HOMO,

HOMO-1 and HOMO-2) and approximate as $t_2$ ($d_{xy}$, $d_{xz}$ and $d_{yz}$), and another two MOs at lower energy (HOMO-4 and HOMO-5) which approximate as e ($d_{x2-y2}$ and $d_{z2}$). The MLCT transition can therefore be said to be $t_2$ to π* (bipyridine) in

**Table 4** Percentage contributions from component parts of **4**, **5**, **7** and **9** to selected molecular orbitals. Also quoted are the calculated energies for these molecular orbitals

| | | | | % Contribution from | | |
|---|---|---|---|---|---|---|
| Complex | MO | MO character | MO energy/eV | Cu-based orbitals | POP-based orbitals | Bpy-based orbitals |
| **4** | HOMO-1 | $d_{xz}$ or $d_{yz}$ | –5.99 | 63.78 | 8.80 | 27.42 |
| | HOMO | $d_{xz}$,or $d_{yz}$ | –5.87 | 44.34 | 50.38 | 5.28 |
| | LUMO | π*-bpy | –2.27 | 1.48 | 5.68 | 92.84 |
| **5** | HOMO-3 | | –6.60 | 14.09 | 83.47 | 2.44 |
| | HOMO-2 | | –6.42 | 38.48 | 54.01 | 7.51 |
| | HOMO | | –6.08 | 36.98 | 58.41 | 4.61 |
| | LUMO | π*-bpy | –3.16 | 2.57 | 4.25 | 93.18 |
| | LUMO+1 | π*-bpy | –2.60 | 0.40 | 0.53 | 99.07 |
| **7** | HOMO-2 | $d_{xy}$ | –6.27 | 51.93 | 38.80 | 9.27 |
| | HOMO-1 | $d_{xz}$,or $d_{yz}$ | –6.03 | 61.10 | 18.98 | 19.92 |
| | LUMO | π*-bpy | –2.12 | 1.44 | 4.24 | 94.32 |
| **9** | HOMO-1 | | –6.33 | 59.87 | 12.00 | 28.13 |
| | HOMO | | –6.07 | 38.12 | 56.37 | 5.51 |
| | LUMO | π*-bpy | –2.92 | 1.47 | 3.80 | 94.73 |
| | LUMO+1 | π*-bpy | –2.27 | 1.97 | 3.41 | 94.62 |

**Table 5** TD-DFT calculated visible absorption wavelengths for **4**, **5**, **7** and **9**, indicating the molecular orbitals involved and their relative contribution to the absorption

| | | Main charge transitions | | |
|---|---|---|---|---|
| Complex | Main visible absorbance/nm | Mo from | MO to | Relative contribution |
| **4** | 416 | HOMO-1 | LUMO | 16% |
| | | HOMO | LUMO | 84% |
| **5** | 509 | HOMO | LUMO | 100% |
| | 420 | HOMO-3 | LUMO | 29% |
| | | HOMO-2 | LUMO | 10% |
| | | HOMO | LUMO+1 | 61% |
| **7** | 402 | HOMO-1 | LUMO | 59% |
| | | HOMO-2 | LUMO | 41% |
| **9** | 481 | HOMO-1 | LUMO | 37% |
| | | HOMO | LUMO | 63% |
| | 383 | HOMO-1 | LUMO+1 | 46% |
| | | HOMO | LUMO+1 | 54% |

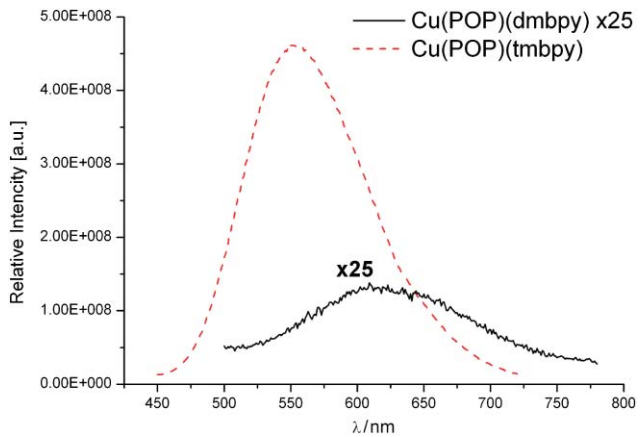


**Fig. 6** Isosurface images generated from DFT calculations of (a) LUMO for **4**; (b) LUMO for **5**.

nature. Despite the lowest energy MLCT transition taking place in **5**, **7** and **9** being of the same character, their MO diagrams vary more from the ideal pseudo-tetrahedral model due to increased interactions with the ligand-based orbitals. Inspection of Table 5 demonstrates that the LUMO and LUMO+1 orbitals for all four of the complexes are bpy-based, and that the HOMO to HOMO-3 orbitals are Cu(I)- and POP-based, as predicted.

This is of importance as the main charge-transfer transitions occur between these orbitals (see Table 5), indicating MLCT across the molecule in the desired direction for DSSC function of the acid analogous: towards the acid groups bound to the $TiO_2$.

### Emission spectroscopy

Excitation and emission spectra were investigated for **4**, **7** and **9** in ethanol at room temperature and in a frozen glass at 77 K. For comparison, data were also collected for the uncomplexed dmbpy and tmbpy ligands, and the precursor complex $[CuPOP(MeCN)_2][BF_4]$ (Table 6).Maxima values are given in Table 6 with full spectra given in the supplementary information. Complex **9** was found to be emissive only at 77 K and not at room temperature. Complexes **4** and **7** both showed room-temperature emission with a significant increase in intensity upon freezing accompanied by some shifting of the absorption and emission maxima (Fig. 7). This behaviour is consistent with emission from a triplet MLCT state in keeping with characteristic behaviour of related Cu(I) polypyridyl complexes.[8]

Fig. 8 shows a comparison of the emission intensity for **4** and **7**, where the excitation wavelengths used for both complexes have comparable molar absorption coefficients. The role of the 6,6′-methyl groups on the bipyridine ligand is apparent in providing additional steric constraint to the complex leading to the significantly greater emission intensity of **7**. Nevertheless, the observation of emission from **4**, **7** and **9**, all of which lack 6,6′-substituents on the bipyridyl, demonstrates the role of the ancilliary POP ligand in providing structural rigidity to the complex. To function as a sensitiser in a DSSC, a complex must possess a sufficiently long excited-state lifetime to enable charge injection into the semiconductor condution band and the observation of photoluminescence is generally taken as an indication that the excited-state lifetime will be sufficiently long. Alonside the structural studies, the observed emission from **4**, **7** and **9** demonstrates the suitability of using the dcbpy ligand in conjuction with a sterically-blocking co-ligand



 

**Table 6** Excitation and emission measurements for dmby, tmbpy, $[CuPOP(MeCN)_2][BF_4]$, **4**, **7**, and **9**

| | Room-temperature EtOH | | 77 K rigid matrix (EtOH) | |
|---|---|---|---|---|
| Compound | Excitation maxima $\lambda_{max}$/nm | Emission maxima $\lambda_{max}$/nm | Excitation maxima $\lambda_{max}$/nm | Emission maxima $\lambda_{max}$/nm |
| dmbpy | 300, 330 | 410 | Not recorded | Not recorded |
| tmbpy | 264, 304 | 373 | Not recorded | Not recorded |
| $CuPOP(MeCN)_2$ | 324 | 457 | Not recorded | Not recorded |
| **4** | 408 | 618 | 340 | 592 |
| **7** | 369 | 554 | 369 | 527 |
| **9** | Not observed | Not observed | 328, 356 | 515 |



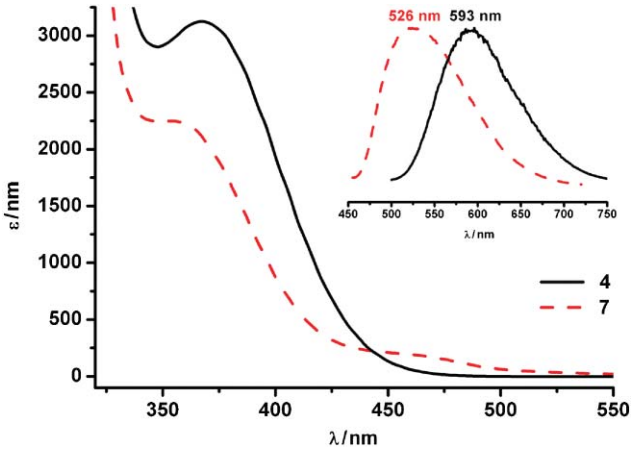


**Fig. 7** Absorbance and emission spectra for heteroleptic complexes **4** and **7**. Absorbance spectrum carried out in MeCN; fluorescence emission spectrum recorded in a rigid matrix of EtOH.

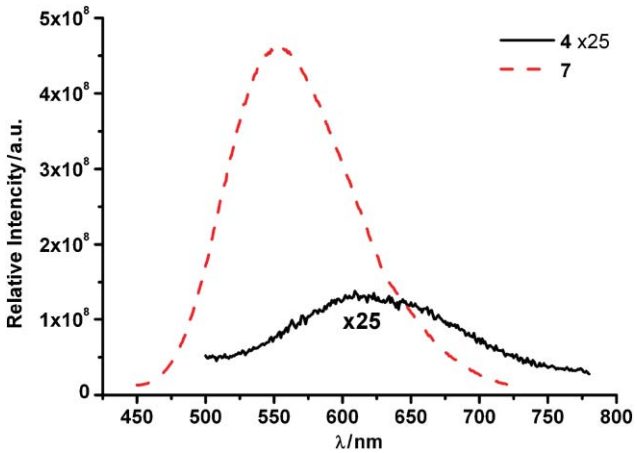


**Fig. 8** Emission spectra for **4** and **7** recorded in EtOH at 300 K. The spectra have been normalised against concentration of solution used.

to design Cu(I) DSSC sensitisers. Due to the qualitatively large photoluminescence observed for **7**, the photophysical properties of complexes **4** and **7** are currently under further investigation in a variety of media and a range of temperatures along with computational studies of structural rigidity in the excited state. This work will be reported elsewhere.

## Electrochemistry

The redox potentials for all complexes are shown in Table 7. The first oxidation potential for the homoleptic complexes occurs within the range +0.75 to +0.91 V and can be assigned as an irreversible Cu(I)/Cu(II) redox process. The corresponding Cu(I)/Cu(II) oxidation for the heteroleptic complexes (**4**–**7**) occurs at more positive potentials, around +1.4 V (Table 7). This increase in Cu(I) oxidation potential is due to the orbital interaction with the electron withdrawing POP ligand.[8] The oxidation potentials vary little across **4**–**7**, suggesting the HOMO is largely Cu(I)/POP in character as this feature is invariant across the series. This is also consistent with the TDDFT results shown in Tables 4 and 5 and is appropriate for use of **5** as a DSSC sensitiser since positive charge density on the oxidised sensitiser will be located away from the semiconductor. For long-term DSSC operation, it would clearly be preferable to develop sensitisers that exhibit chemically reversible oxidations, however the acid analogue, **5**, is still viable for study as model sensitiser since cyclic voltammetry experiments occur on a far longer timescale relative to those taking place in a DSSC device.

**Table 7** Oxidation and reduction potentials for all complexes; **1**, **4**–**7** and **9** = 0.3M $TBABF_4$/MeCN; **3** = 0.3M $TBABF_4$/DCM

| | | $E_{\frac{1}{2}}$ (V *vs.* Ag/AgCl) | | | | | | | |
|---|---|---|---|---|---|---|---|---|---|
| Complex | | $E_{Red.4}$ | $E_{Red.3}$ | $E_{Red.2}$ | $E_{Red.1}$ | $E_{Ox.1}$ | $E_{Ox.2}$ | $E_{Ox.3}$ | $E_{Ox.4}$ |
| $[Cu(tmbpy)_2]$ | **1** | | | −1.68 | −1.34 | +0.77 | | | |
| $[Cu(tecbpy)_2]$ | **3** | | | −1.27 | −0.87 | +0.91* | | | |
| [CuPOP(dmbpy)] | **4** | | | | −1.60 | +1.44 | +1.73 | | |
| [CuPOP(dcbpy)] | **5** | | | −1.61 | −1.40 | +1.41 | +1.64 | | |
| [CuPOP(decbpy)] | **6** | | | −1.52 | −0.91 | +1.42 | +1.68 | | |
| [CuPOP(tmbpy)] | **7** | | | | −1.66 | +1.41 | +1.65 | | |
| [CuPOP(bpym)] | **9** | −1.63 | −1.44 | −1.08 | −0.78* | +0.55* | +1.24 | +1.44 | +1.75 |

All potentials *vs.* Ag/AgCl (saturated solution); recorded at 298 K; Peaks are chemically and electrochemically irreversible and values shown represent peak potential, except; * = Peaks are chemically reversible and electrochemically irreversible, and values shown represent $E_{\frac{1}{2}}$.

**Table 8** *I–V* Characterisation data for **5**. Dye Bath diethyl ether. Adsorption time 24 h. $V_{OC}$ = open circuit potential, $I_{SC}$ = short circuit current, ff = fill factor, $\eta$ = power conversion efficiency. N719 measure $I_{SC}$ = 7.96 mA; $V_{OC}$ = 753 mV; ff = 0.51 and $\eta$ = 3.05%

| Dye concentration/mM | Cheno concentration/mM | Post-treated with $TiCl_4$ | $I_{SC}$/mA | $V_{OC}$/mV | ff | $\eta$/% |
|---|---|---|---|---|---|---|
| 1 | N/A | N | 0.176 | 361 | 0.51 | 0.032 |
| 2 | N/A | N | 0.233 | 347 | 0.65 | 0.053 |
| 1 | 1 | N | 0.198 | 333 | 0.48 | 0.030 |
| 2 | 2 | N | 0.300 | 373 | 0.45 | 0.050 |
| 1 | N/A | Y | 0.210 | 388 | 0.47 | 0.038 |
| 2 | N/A | Y | 0.230 | 345 | 0.58 | 0.046 |



Upon comparison with literature,[1] the reductions exhibited by all the complexes can be assigned as bipyridyl-ligand based, which is consistent with the predictions from TDDFT. The variation in reduction potential seen for the complexes is consistent with their calculated LUMO energies, with the acid and ester analogues requiring a less negative reduction potential due to the extended conjugation. These electrochemical results support the expectation that the charge transfer transition will have directionality in the desired direction; towards the carboxylate groups (on the bipyridyl ligand) that bind to $TiO_2$.

### Solar cell measurements

*I–V* characterisation was carried out on solar cells made using **5** adsorbed onto $TiO_2$ films. Cell construction and treatments are outlined in the Experimental section and power-conversion efficiency was determined while irradiating under AM 1.5 light (100 $mWcm^{-2}$). Cell efficiencies ($\eta$) were calculated using the resulting values of $I_{SC}$ = short circuit current (mA), $V_{OC}$ = open circuit voltage (mV) and ff = fill factor.

Adsorption studies revealed the dye bath conditions yielding the optimum $TiO_2$ surface coverage of **5** to be a sensitiser concentration of 2 mM in diethyl ether. The results for 1 mM diethyl ether dye baths have also been quoted for completeness. Approximate relative $TiO_2$ surface coverage was determined using UV/Vis spectroscopy. This method also allowed confirmation that the dye bound without degradation by comparison with the absorption spectra of **5** in solution. Results for a selected range of these cells are shown in Table 8 and for comparative reasons, N719 DSSCs were constructed and tested following the same procedures.

The observed photovoltages for cells using complex **5** were consistently around 350 mV, lower than that observed for N719 (753 mV), and lower than the best homoleptic Cu(I) sensitisers quoted in the literature (around 550 mV),[2,3,5–7] The photocurrents were also significantly lower than those recorded for our N719 cells and for existing homoleptic

Cu(I) sensitisers (up to 0.3 mA compared to 8.0 and 5.0 mA respectively). This however is as expected due to the blue shift of the MLCT absorption caused by the electron-accepting POP ligand such that the complex only just absorbs in the visible region ($\lambda_{max}$ = 394 nm). The low photocurrents may also play a role in the reduced photovoltages displayed using this sensitiser.

The studies reported in Table 8 include two additional DSSC fabrication procedures outlined in the literature. Firstly, the inclusion of Chenodeoxycholic acid (Cheno) in the dye baths was carried out as it has been shown to dramatically improve the short circuit currents produced in some systems[36–40] by acting as a spacer group on the $TiO_2$ surface, limiting the extent of dye aggregation. A range of dye:Cheno concentration ratios were tried for **5** with representative examples in Table 8. Improved photocurrents for the dye:Cheno cells over the non-Cheno cells was observed in every case, with an optimum ratio of 1 : 1, although no improvement to the photovoltage was seen. Secondly, a $TiCl_4$ post-treatment of the $TiO_2$ film prior to adsorption of the sensitiser was applied as a potential method for improving photocurrents.[9,40] No improvement to photocurrent was recorded upon the introduction of the $TiCl_4$ post-treatment, and photovoltages remained within the same range seen throughout this work (Table 8).

Despite the low power-conversion efficiency of cells sensitised with **5**, the key feature of the work is the demonstration of sensitiser function for a dye of this design. The POP ligand was chosen for its known steric rigidity and successfully demonstrates that simple dcbpy ligands can be used in heteroleptic Cu(I) DSSC sensitisers due to the chemical stability and sufficiently-long excited-state lifetime imposed by the POP. The low power-conversion efficiency is largely the result of poor harvesting of the solar spectrum by the dye leading to low $I_{SC}$. Our future work is now focused on the development of sterically-constraining co-ligands that also impart more optimised spectroscopic characteristics on heteroleptic Cu(I) DSSC sensitisers.

## Conclusions

Shown here is the synthesis of a series of homoleptic complexes of general formula $[Cu(I)(diimine)_2][BF_4]$ (**1**–**3**), and a series of heteroleptic complexes of the general formula $[Cu(I)(POP)(diimine)][BF_4]$ (**4**–**9**). Electrochemical, spectroscopic and computational methods were used to understand the electronic characteristics of these complexes. In particular, this work demonstrates the first example of a heteroleptic Cu(I) complex; $[Cu(I)(POP)(dcbpy)][BF_4]$ (**5**), that functions as a sensitiser in a dye-sensitised solar cell. The photocurrents and photovoltages achievable by **5** are lower than existing Cu(I)-sensitisers[7] but this is a result of the dye absorbing weakly in the visible region ($\lambda_{max}$ = 394 nm and $\varepsilon_{max} = 3.3 \times 10^3$ $M^{-1}cm^{-1}$).

A key point of this work is that stable heteroleptic Cu(I)-sensitisers can be achieved with simple 4,4′($CO_2H$)-bipyridine, synthetically less intensive to produce than the 4,4′,6,6′-substituted analogues. Work is now moving towards replacing the POP ligand with a more suitable second ligand that can have a beneficial impact on the absorption properties of the sensitiser as well as providing the required steric constraint.

 

## Experimental

### General procedures

The synthesis of bis{2-(diphenylphosphanyl)phenyl} ether (POP),[8] 4,4′-dicarboxy-2,2′-bipyridine (dcbpy),[41] 4,4′-di($CO_2$Et)-2,2′-bipyridine (decbpy),[42] 4,4′,6,6′-tetramethyl-2,2′-bipyridine (tmbpy),[43] [Cu(MeCN)$_4$][$BF_4$][44] and [Cu(I)POP(MeCN)$_2$][$BF_4$][8] were carried out according to literature procedures. 4,4′,6,6′-tetracarboxy-2,2′-bipyridine (tcbpy) and 4,4′,6,6′-tetra($CO_2$Et)-2,2′-bipyridine (tecbpy) are novel complexes and have been synthesized using adapted literature methods.[42]

4,4′-dimethyl-2,2′-bipyridine (dmbpy), bipyrimidine (bpym) and all other chemicals were purchased from Aldrich and used as received.

Electrochemistry was carried out using a Pt working electrode, Pt rod counter electrode and Ag/AgCl reference electrode. All electrochemical experiments were carried out in either acetonitrile or DCM and the supporting electrolyte used was $TBABF_4$ (0.3M). After each experiment the reference electrode was calibrated against the ferrocene/ferrocenium couple which was found to be at 0.55 V. The absorption spectra were recorded using a PerkinElmer Lambda 9 spectrophotometer controlled using the UV/Winlab software. Emission spectra were recorded at room temperature and using frozen samples, with ethanolic solutions of **4**, **7**, **9**, [CuPOP(MeCN)$_2$][$BF_4$], dmbpy and tmbpy (0.1–0.6 mM), using a Fluoromax2 fluorimeter controlled by the ISAMain software.

Density functional theory calculations were performed using the Gaussian 03 program[29] with the starting structures for **4**, **5** and **7** inputted using the builder program Arguslab and the crystal structure coordinates used as the starting point for **9**. All calculations were carried out using the Becke's three parameter exchange functional with the Lee–Yang–Parr for the correlation functional (B3LYP),[30] using the Los Alamos National Laboratory basis sets, known as LANL2DZ (developed by Hay and Wadt),[31–33] which comprises ECP + double zeta for copper, and the all-electron valence double zeta basis sets developed by Dunning (D95V) for light atoms.[45] Frequency calculations were carried out to ensure that optimised geometries were minima on the potential energy surface. Solvent effects were included *via* the self-consistent reaction field (SCRF) method using the polarised continuum model (PCM),[46] with slight modifications to the default cavity parameters to aid convergence. Time-dependent density functional theory (TDDFT) was performed in an acetonitrile polarizable continuum model, with the first 70 singlet transitions calculated. ArgusLab[34] was used to generate the orbital isosurface maps.

To make the DSSCs titanium dioxide paste (Dyesol, DSL-18NR-T) was deposited onto cleaned fluorine doped tin oxide conductive glass (TEC 8, Pilkington, UK) by doctor-blading. The film was dried at 100 °C for 15 min and then sintered at 450 °C for 30 min to remove the organics and to form a mesoporous film structure. The thickness of the film was about 18 μm. The films were sensitized with **5** using a solution of the dye in diethyl ether. The platinized counter electrode was fabricated following the previously reported procedure.[47] The cell was completed by sealing the dye coated $TiO_2$ electrode and Pt electrode of a cell together by a thermal plastics spacer (Surlyn 1702, 25 μm, Solaronix) at 120 °C. The electrolyte was introduced into the cell through the two holes which were drilled in the counter electrode. The holes were subsequently sealed using Kapton tape. The default electrolyte used was 0.6 M LiI, 0.03 M $I_2$, 0.1 M Guanidinium thiocyanate, 0.5 M 4-*tert*-butylpyridine, 15 : 85 Valeronitrile:Acetonitrile. The active area of the cell was 1 $cm^2$. The current–voltage characteristics of the cells were measured under simulated AM 1.5 illumination (100 $mWcm^{-2}$) provided by a solar simulator (1 kW Xe with AM 1.5 filter, Müller) calibrated using a Digital Solar Power Meter. The Cheno additive was dissolved in the Dye Baths at the same time as the sensitiser. The $TiCl_4$ post-treatment of the $TiO_2$ films was carried out prior to dye adsorption. The $TiO_2$ coated FTO cells were coated with a 40mM aqueous $TiCl_4$ solution and placed into a steam bath at 70 °C for 30 min. The cells were removed, washed with deionised water, dried at 100 °C for 15 min and then sintered at 500 °C for 30 min. Dye adsorption was then carried out as described above.

#### Cu(tmbpy)$_2$][$BF_4$] (1)

[Cu(MeCN)$_4$][$BF_4$] (140 mg, 0.45 mmol) and tmbpy (200 mg, 0.89 mmol) were stirred in 20 mL degassed chloroform under nitrogen for 30 min. The solvent was removed under reduced pressure and the solid obtained triturated in hexane. The product was obtained by filtration. Yield = 75%, 193 mg. $\delta_H$ (DMSO, 250 MHz)/ppm = 8.36 (s, 4H, H-bpy), 7.42 (s, 4H, H-bpy), 2.45 (s, 12H, $CH_3$), 2.11 (s, 12H, $CH_3$). MS (positive ESI); *m*/*z*: 487.10 (M–$BF_4^-$)$^+$. Elemental analysis: calculated for $C_{28}H_{32}BCuF_4N_4$: C 58.49, H 5.61, N 9.74. Found: C 57.78, H 5.46, N 9.57.

#### [Cu(tcbpy)$_2$][$BF_4$] (2)

[Cu(MeCN)$_4$][$BF_4$] (20.5 mg, 0.07 mmol) and tcbpy (42.3 mg, 0.13 mmol) were stirred in 5 mL degassed, dry MeOH under nitrogen for 2 h. A white solid (uncomplexed tcbpy) was removed by filtration. The pure product was then obtained by precipitation with isopropyl alcohol overnight. Yield = 32%, 17 mg. $\delta_H$(DMSO, 250 MHz)/ppm: 8.84 (s, 4H, H-bpy), 8.22 (s, 4H, H-bpy). MS (positive ESI): *m*/*z* = 725.31 (M–$BF_4^-$)$^+$. Elemental analysis: calculated for $C_{28}H_{16}BCuF_4N_4O_{16}$: C 41.27, H 1.98, N 6.88. Found: C 41.44, H 2.24, N 7.96.

#### [Cu(tecbpy)$_2$][$BF_4$] (3)

[Cu(MeCN)$_4$][$BF_4$] (14.2 mg, 0.05 mmol) and tecbpy (40 mg, 0.09 mmol) were stirred in 50 mL degassed, dry DCM under nitrogen for 30 min. The pure product was obtained by precipitation with isopropyl alcohol. Yield = 53%, 28 mg. $\delta_H$ ($CDCl_3$, 250 MHz)/ppm = 9.15 (s, 4H, H-bpy), 8.69 (s, 4H, H-bpy), 4.54 (q, *J* = 7.10 Hz, 8H, –C**H$_2$**–$CH_3$), 3.88 (q, *J* = 7.14 Hz, 8H, –C**H$_2$**–$CH_3$), 1.47 (t, *J* = 7.18 Hz, 12H, –$CH_2$–C**H$_3$**), 1.03 (t, *J* = 7.11 Hz, 12H, $CH_2$–C**H$_3$**). MS (positive ESI); *m*/*z*: 950 (M–$BF_4^-$)$^+$. Elemental analysis: calculated for $C_{44}H_{48}N_4O_{16}CuBF_4{\cdot}CH_2Cl_2$: C 48.08, H 4.48, N, 4.98. Found: C 47.60, H 4.33, N 4.79.

#### [Cu(POP)(dmbpy)][$BF_4$] (4)

[Cu(I)POP(MeCN)$_2$][$BF_4$] (201 mg, 0.26 mmol) and dmbpy (51 mg, 0.06 mmol) were stirred in 5 mL acetone for 3 h resulting in an orange solution. The solvent was removed under reduced pressure. The pure product was then obtained by reprecipitaiton

**Table 9** X-Ray crystallography data

| | [Cu(dmbpy)$_2$Cl] [BF$_4$] | **1** | **6** | **9** | **10** |
|---|---|---|---|---|---|
| CCDC deposition number | 771442 | 771443 | 771439 | 771440 | 771441 |
| Empirical Formula | $(C_{24}H_{24}N_4CuCl)_2$. $(BF_4)_2\cdot(CH_2Cl_2)$ | $C_{28}H_{32}N_4Cu\cdot BF_4$ | $C_{52}H_{44}N_2CuO_5P_2$ $BF_4\cdot C_2H_3N$ | $C_{44}H_{34}N_4OP_2Cu\cdot BF_4$ | $C_{80}H_{62}N_4O_2P_4Cu_2\cdot 2[BF_4]\cdot 2[C_3H_6O]$ |
| Formula weight | 1193.47 | 574.93 | 1030.24 | 847.08 | 1652.15 |
| $T$/K | 150(2) | 150(2) | 100(2) | 150(2) | 150(2) |
| Crystal colour | Cyan | Orange | Orange | Orange | Orange-Yellow |
| Crystal dimensions | 0.50 × 0.40 × 0.30 | 0.90 × 0.59 × 0.43 | 0.15 × 0.15 × 0.08 | 0.22 × 0.33 × 0.36 | 0.15 × 0.21 × 0.25 |
| Crystal system | Triclinic | Monoclinic | Triclinic | Monoclinic | Triclinic |
| Space group | $P\bar{1}$ | $C2/c$ | $P\bar{1}$ | $P2_1/c$ | $P\bar{1}$ |
| $a$/Å | 10.8528(3) | 13.8531(14) | 12.3345(3) | 9.5405(2) | 11.3321(3) |
| $b$/Å | 14.4072(4) | 16.4771(14) | 12.6111(3) | 19.8580(4) | 13.2821(3) |
| $c$/Å | 17.6085(5) | 13.5039(19) | 18.0200(4) | 20.4442(4) | 14.2188(3) |
| $\alpha$ (°) | 83.9868(16) | 90 | 98.4411(13) | 90 | 108.665(1) |
| $\beta$ (°) | 74.9744(14) | 119.730(7) | 100.4738(12) | 95.4810(10) | 105.605(1) |
| $\gamma$ (°) | 73.3850(14) | 90 | 113.2549(12) | 90 | 97.186(1) |
| $V$/Å$^3$ | 2546.69(12) | 2676.7(5) | 2457.18(10) | 3855.55(14) | 1899.81(7) |
| $Z$ | 4 | 4 | 2 | 4 | 1 |
| $D_c$/Mg m$^{-3}$ | 1.556 | 1.427 | 1.392 | 1.459 | 1.440 |
| Independent reflections | 8998 [$R_{int}$ = 0.0411] | 2747 [$R_{int}$ = 0.0492] | 10570 [$R_{int}$ = 0.0606] | 10239 [$R_{int}$ = 0.038] | 10287 [$R_{int}$ = 0.037] |
| All data/restraints/parameters | 36169/0/666 | 13995/184/190 | 49789/63/680 | 31367/0/514 | 27104/0/496 |
| Absorption correction/mm$^{-1}$ | 1.119 | 0.869 | 0.577 | 0.711 | 0.719 |
| $R_1$, w$R_2$ (observed data: $F^2>2\sigma(F^2)$) | 0.0366/0.0933 | 0.0526/0.1470 | 0.0422/0.0937 | 0.0485/0.1071 | 0.0537/0.1160 |



from acetonitrile upon addition of isopropyl alcohol and leaving overnight. Yield = 67%, 153 mg. $\delta_H$(DMSO, 250 MHz)/ppm:. 8.51 (s, 2H, H-bpy), 8.37 (d, 2H, H-bpy), 7.47-7.15 (m, 18H, H-POP), 7.09 (t, 2H, H-bpy), 6.98 (m, 8H, H-POP), 6.61 (m, 2H, H-POP), 2.47 (s, 6H, $CH_3$-bpy). MS (positive FAB): $m/z$ = 784.7 (M–$BF_4^-$)$^+$. Elemental analysis: calculated for $C_{48}H_{40}BCuF_4N_2OP_2$: C 66.03, H 4.62, N 3.21. Found: C 65.58, H 4.42, N 3.90.

### [Cu(POP)(dcbpy)][BF$_4$] (5)

[Cu(I)POP(MeCN)$_2$][BF$_4$] (100 mg, 0.13 mmol) and dcbpy (28 mg, 0.03 mmol) were stirred in 5 mL acetone for 3 h resulting in a yellow solution. The pure product was then obtained by reprecipitation upon addition of isopropyl alcohol and leaving overnight. Yield = 26%, 96 mg. $\delta_H$(DMSO, 250 MHz)/ppm: 9.17 (s, 2H, H-bpy), 8.91 (d, 2H, H-bpy), 8.07 (d, 2H, H-bpy), 7.4 (m, 28H, H-POP). MS (positive ESI): $m/z$ = 844.80 (M–$BF^-$)$^+$. Elemental analysis: calculated for $C_{48}H_{36}CuN_2O_5P_2.BF_4$: C 61.73, H 3.89, N 3.00. Found C 62.06, H 4.20, N 2.87.

### [Cu(POP)(decbpy)][BF$_4$] (6)

[Cu(I)POP(MeCN)$_2$][BF$_4$] (201 mg, 0.26 mmol) and decbpy (51 mg, 0.05 mmol) were stirred in 5 mL acetone for 3 h resulting in an orange solution. The solvent was removed under reduced pressure. The pure product was then obtained by reprecipitation upon addition of isopropyl alcohol and leaving overnight. Yield = 87%. 231 mg, $\delta_H$(DMSO, 250 MHz)/ppm: 8.79 (s, 2H, H-bpy), 8.75 (d, $J$ = 4.74 Hz, 2H, H,-bpy), 7.98 (dd, $J$ = 1.32 Hz, $J$ = 5.42 Hz, 2H, H-bpy), 7.10 (m, 28H, H-POP), 4.53 (dd, $J$ = 7.07 Hz, 4H, C**H$_2$**CH$_3$), 1.49 (t, $J$ = 7.13 Hz, 6H, CH$_2$C**H$_3$**). MS (positive ESI): $m/z$ = 784.87 (M–$BF^-$)$^+$. Elemental analysis: calculated for $C_{52}H_{44}CuN_2O_5P_2.BF_4$: C 63.14, H 4.48, N 2.83. Found C 62.71, H 4.36, N 2.11.

### [Cu(POP)(tmbpy)][BF$_4$] (7)

[Cu(I)POP(MeCN)$_2$][BF$_4$] (101 mg, 0.13 mmol) and tmbpy (25 mg, 0.03 mmol) were stirred in 10 mL anhydrous acetonitrile under $N_2$ for 3 h resulting in an orange solution. The volume of reaction mixture was reduced by half under reduced pressure. The pure product was then obtained upon addition of isopropyl alcohol and leaving overnight. The desired product remains in the filtrate and is obtained by solvent removal under reduced pressure. Yield = 75%, 90 mg. $\delta_H$(DMSO, 250 MHz)/ppm: 8.09 (s, 2H, H-bpy), 6.85-7.34 (m, 30H, H-bpy and POP), 2.37 (s, 6H, $CH_3$), 2.31 (s, 6H, $CH_3$). MS (positive FAB): $m/z$ (%) = 812.6 (M–$BF^-$)$^+$. Elemental analysis: calculated for $C_{50}H_{44}BCuF_4N_2OP_2$: C 66.64, H 4.92, N 3.11. Found C 66.40, H 4.76, N 3.00.

### [Cu(POP)(tcbpy)][BF$_4$] (8)

[Cu(I)POP(MeCN)$_2$][BF$_4$] (100 mg, 0.13 mmol) and tcbpy (45 mg, 0.04 mmol) were stirred in 5 mL acetone for 3 h resulting in a dark purple solution and white solid. The white solid was removed by filtration. The pure product was then obtained by reprecipitation upon addition of isopropyl alcohol and leaving overnight. The desired product remains in the filtrate and was obtained by solvent removal under reduced pressure. Yield = 53%, 72 mg. $\delta_H$(DMSO, 250 MHz)/ppm: 9.32 (s, 2H, H-bpy), 8.72 (s, 2H, H-bpy), 6.87-7.67 (m, 28H, POP). MS (positive FAB): $m/z$ (%) = 617.3 (CuPOP). Elemental analysis: calculated for $C_{50}H_{36}BCuF_4N_2O_9P_2$: C 58.81, H 3.55, N 2.74. Found C 59.10, H 3.88, N 2.86.

### [Cu(POP)(bpym)][BF4] (9)

[Cu(I)POP(MeCN)$_2$][BF4] (486 mg, 0.63 mmol) and bpym (100 mg, 0.63 mmol) were stirred in 20 mL DCM. The product was obtained by concentration of the reaction mixture then precipitation by the addition of ether. Yield = 64%.

 

$\delta_H$($CD_3OD$, 250 MHz)/ppm: 8.90 (s, 4H, H-bpym), 7.59–6.77 (m, 30H, H-bpym and H-POP). Elemental analysis: calculated for $C_{44}H_{34}BCuF_4N_4OP_2$: C 62.39, H 4.05, N 6.61. Found C 61.56, H 3.43, N 6.34

**$[Cu_2(POP)_2(\eta 4\text{-bpym})][(BF_4)_2]$ (10)**

[Cu(I)POP($MeCN)_2$][BF4] (33 mg, 0.04 mmol) and **11** (34 mg, 0.04 mmol) were stirred in 5 mL acetone for 30 h. The product was obtained by concentration of the reaction mixture then precipitation by the addition of ether. Despite obtaining a crystal structure we were unable to obtain a pure product with satisfactory elemental analysis. Yield = 48%, 32 mg. $\delta_H$(DMSO, 250 MHz)/ppm: 9.01 (s, 4H, H-bpym), 7.85-6.58 (m, 58H, H-bpym and H-POP). Elemental analysis: calculated for $C_{80}H_{62}B_2Cu_2F_8N_4O_2P_4$: C 62.56, H 4.07, N 3.65. Found C 59.06, H 3.96, N 3.01.

### X-ray crystallography

Crystals of [Cu($dmbpy)_2$][$BF_4$] were grown by slow diffusion of diethyl ether into a saturated DCM solution of **4**. Crystals of **1** and **9** were grown by slow diffusion of diethyl ether into a saturated DCM solution of **1** or **9** respectively. Crystals of **6** were grown by slow diffusion of diethyl ether into a saturated solution of **6** in acetonitrile. Crystals of **10** was grown by slow diffusion of hexane into a saturated solution of **10** in acetone. Single crystal X-ray diffraction data are given in Table 9 and were collected using Mo-K$\alpha$ radiation ($\lambda$ = 0.71073 Å) on a Smart APEX CCD diffractometer equipped with an Oxford Cryosystems low-temperature device operating at 150 K. An absorption correction was applied using the multi-scan procedure SADABS.[48] The structures were solved by Direct methods (Shelx[49] for [Cu($dmbpy)_2$][$BF_4$], **1** and **6**; and SIR92[50] for **9** and **10**) and refined by full-matrix least squares against $|F|^2$ using all data (Shelx[49] for [Cu($dmbpy)_2$][$BF_4$], **1** and **6**; and CRYSTALS[51] for **9** and **10**). Figures were prepared using the programme Mercury.[52] All non-H atoms were refined with anisotropic displacement parameters.

## Acknowledgements

We thank EaSTChem and the EPSRC Supergen Excitonic Solar Cell Consortium for funding. This work has made use of the resources provided by the EaStChem Research Computing Facility (http://www.eastchem.ac.uk/rcf). This facility is partially supported by the eDIKT initiative (heep://www.edikt.org).

## Notes and references

1 N. Armaroli, *Chem. Soc. Rev.*, 2001, **30**, 113.
2 N. Alonso-Vante, J.-F. Nierengarten and J.-P. Sauvage, *J. Chem. Soc., Dalton Trans.*, 1994, 1649.
3 S. Sakaki, T. Kuroki and T. Hamada, T., *J. Chem. Soc., Dalton Trans.*, 2002, 840.
4 A. Barbieri, G. Accorsi and N. Armaroli, *Chem. Commun.*, 2008, 2185.
5 T. Bessho, E. C. Constable, M. Graetzel, A. H. Redondo, C. E. Housecroft, W. Kylberg, Md. K. Nazeeruddin, M. Neuburger and S. Schaffner, *Chem. Commun.*, 2008, 3717.
6 A. Hernandez Redondo, E. C. Constable and C. E. Housecroft, *Chimia*, 2009, **63**, 205.
7 E. C. Constable, A. H. Redondo, C. E. Housecroft, M. Neuburger and S. Schaffner, *Dalton Trans.*, 2009, 6634.
8 N. Armaroli, G. Accorsi, M. Holler, O. Moudam, J.-F. Nierengarten, Z. Zhou, R. T. Wegh and R. Welter, *Adv. Mater.*, 2006, **18**, 1313.
9 M. K. Nazeeruddin, A. Kay, I. Rodicio, R. Humphry-Baker, E. Mueller, P. Liska, N. Vlachopoulos and M. Grätzel, *J. Am. Chem. Soc.*, 1993, **115**, 6382.
10 http://www.g24i.com/.
11 N. Robertson, *Angew. Chem., Int. Ed.*, 2006, **45**, 2338.
12 C. L. Linfoot, P. Richardson, K. L. McCall, J. R. Durrant, A. Morandeira and N. Robertson, *Solar Energy*, in press.
13 S. Ferrere and B. Gregg, *J. Am. Chem. Soc.*, 1998, **120**, 843.
14 S.-M. Kuang, D. G. Cuttell, D. R. Mcmillin, P. E. Fanwick and R. A. Walton, *Inorg. Chem.*, 2002, **41**, 3313.
15 S. Ferrere, *Chem. Mater.*, 2000, **12**, 1083.
16 S. Ferrere, *Inorg. Chim. Acta*, 2002, **329**, 79.
17 N. Robertson, *ChemSusChem*, 2008, **1**, 977.
18 L. Spiccia, G. B. Deacon and C. M. Kepert, *Coord. Chem. Rev.*, 2004, **248**, 1329.
19 R. M. Williams, L. D. Cola, F. Hartl, J.-J. Lagref, J.-M. Planeix, A. D. Cian and M. W. Hosseini, *Coord. Chem. Rev.*, 2002, **230**, 253.
20 N. Armaroli, G. Accorsi, F. Cardinali and A. Listorti, *Photochemistry and Photophysics of Coordination Compounds I*, 69, Springer, 2007.
21 M. Schmitted, C. Michel, S. -X. Liu, D. Schildbach and D. Fenske, *Eur. J. Inorg. Chem.*, 2005, **5**, 1155.
22 M. Ruthkosky, C. A. Kelly, F. N. Castellano and G. J. Meyer, *Coord. Chem. Rev.*, 1998, **171**, 309.
23 O. Moudam, A. Kaeser, B. Delavaux-Nicot, C. Duhayon, M. Holler, G. Accorsi, N. Armaroli, I. Séguy, J. Navarro, P. Destruel and J.-F. Nierengarten, *Chem. Commun.*, 2007, 3077.
24 T. McCormick, W. L. Jia and S. Wang, *Inorg. Chem.*, 2006, **45**, 147.
25 L. Yang, J.-K. Feng, A.-M. Ren, M. Zhang, Y.-G. Ma and X.-D. Liu, *Eur. J. Inorg. Chem.*, 2005, 1867.
26 Y.-M. Xie and J.-H. Wu, *Inorg. Chem. Commun.*, 2007, **10**, 1561.
27 U. Monkowius, Y. N. Svartsov, T. Fischer, M. Zabel and H. Yersin, *Inorg. Chem. Commun.*, 2007, **10**, 1473.
28 Q. Zhang, J. Ding, Y. Cheng, L. Wang, Z. Xie, X. Jing and F. Wang, *Adv. Funct. Mater.*, 2007, **17**, 2983.
29 M. J. Frisch, G. W. Trucks, H. B. Schlegel, G. E. Scuseria, M. A. Robb, J. R. Cheeseman, J. A. Montgomery Jr., T. Vreven, K. N. Kudin, J. C. Burant, J. M. Millam, S. S. Iyengar, J. Tomasi, V. Barone, B. Mennucci, M. Cossi, G. Scalmani, N. Rega, G. A. Petersson, H. Nakatsuji, M. Hada, M. Ehara, K. Toyota, R. Fukuda, J. Hasegawa, M. Ishida, T. Nakajima, Y. Honda, O. Kitao, H. Nakai, M. Klene, X. Li, J. E. Knox, H. P. Hratchian, J. B. Cross, V. Bakken, C. Adamo, J. Jaramillo, R. Gomperts, R. E. Stratmann, O. Yazyev, A. J. Austin, R. Cammi, C. Pomelli, J. W. Ochterski, P. Y. Ayala, K. Morokuma, G. A. Voth, P. Salvador, J. J. Dannenberg, V. G. Zakrzewski, S. Dapprich, A. D. Daniels, M. C. Strain, O. Farkas, D. K. Malick, A. D. Rabuck, K. Raghavachari, J. B. Foresman, J. V. Ortiz, Q. Cui, A. G. Baboul, S. Clifford, J. Cioslowski, B. B. Stefanov, G. Liu, A. Liashenko, P. Piskorz, I. Komaromi, R. L. Martin, D. J. Fox, T. Keith, M. A. Al-Laham, C. Y. Peng, A. Nanayakkara, M. Challacombe, P. M. W. Gill, B. Johnson, W. Chen, M. W. Wong, C. Gonzalez and J. A. Pople, 2004, *Gaussian 03, Revision C.02*, Gaussian, Inc., Wallingford, CT.
30 A. D. Becke, *J. Chem. Phys.*, 1993, **98**, 5648.
31 W. R. Wadt and P. J. Hay, *J. Chem. Phys.*, 1985, **82**, 270.
32 W. R. Wadt and P. J. Hay, *J. Chem. Phys.*, 1985, **82**, 284.
33 W. R. Wadt and P. J. Hay, *J. Chem. Phys.*, 1985, **82**, 299.
34 Arguslab 4.0, M. A. Thompson, *Planaria*, Software LLC, Seattle, http://www.arguslab.com.
35 K. L. McCall, J. R. Jennings, H. Wang, A. Morandeira, L. M. Peter, J. R. Durrant, L. J. Yellowlees, J. D. Woollins and N. Robertson, *J. Photochem. Photobiol. A–Chem.*, 2000, **202**, 196.
36 S. Ito, H. Miura, S. Uchida, M. Takata, K. Sumioka, P. Liska, P. Comte, P. Péchy and M. Grätzel, *Chem. Commun*, 2008, 5194.
37 R. Chen, X. Yang, H. Tian, X. Wang, A. Hagfeldt and L. Sun, *Chem. Mater.*, 2007, **19**, 4007.
38 H. Choi, J. K. Lee, K. H. Song, K. Song, S. O. Kanga and J. Koa, *Tetrahedron*, 2007, **63**, 1553.
39 K. Sayama, S. Tsukagoshi, T. Mori, K. Hara, Y. Ohga, A. Shinpou, Y. Abe, S. Suga and H. Arakawa, *Sol. Energy Mat. Sol. C.*, 2003, **80**, 47.
40 J. H. Yum, S. Moon, R. Humphry-Baker, P. Walter, T. Geiger, F. Nüesch, M. Grätzel and M. K. Nazeeruddin, *Nanotechnology*, 2008, **19**, 424005.

41 P. G. Hoertz, A. Staniszewski, A. Marton, G. T. Higgins, C. D. Incarvito, A. L. Rheingold and G. J. Meyer, *J. Am. Chem. Soc.*, 2006, **128**, 8234.
42 F. H. Case, *J. Am. Chem. Soc.*, 1946, **68**, 2574.
43 P. Ghosh and T. G. Spiro, *J. Am. Chem. Soc.*, 1980, **102**, 5543.
44 O. Moudam, *Thesis*, LCC-Toulouse, France, July 2007.
45 T. H. Dunning Jr. and P. J. Hay, in *Modern Theoretical Chemistry*, Ed. H. F. Schaefer III, Vol. 3 (Plenum, New York, 1976) 1–28.
46 A. Vleck and S. Zalis, *Coord. Chem. Rev.*, 2007, **251**, 258.
47 N. Papageorgiou, W. F. Maier and M. Grätzel, *J. Electrochem. Soc.*, 1997, **144**, 876.
48 G. M. Sheldrick, *SADABS*, Version 2004/1, University of Gottingen, Germany.
49 G. M. Sheldrick, *Acta Cryst.*, 2008, **A64**, 112.
50 A. Altomane, G. Cascarano, C. Giacovazzo, A. Guagliardi, M. C. Burla, G. Polidori and M. Carnalli, *J. Appl. Cryst*, 1994, **27**, 435.
51 P. W. Betteridge, J. R. Carruthers, R. I. Cooper, K. Prout and D. J. Watkin, *J. Appl. Cryst*, 2003, **36**, 1487.
52 C. F. Macrae, P. R. Edgington, P. McCabe, E. Pidcock, G. P. Shields, R. Taylor, M. Towler and J. van de Streek, *J. Appl. Cryst.*, 2006, **39**, 453.



 